

Supporting Information

Preparation and enzymatic application of flower-like hybrid microcapsules by biomimetic mineralization approach

Jiafu Shi,^{a,b,c,†} Shaohua Zhang,^{a,c,†} Xiaoli Wang,^{a,c} Chen Yang,^{a,c} Zhongyi Jiang^{*a,c,d}

^a *Key Laboratory for Green Chemical Technology of Ministry of Education, School of Chemical Engineering and Technology, Tianjin University, Tianjin 300072, China.*

^b *School of Environmental Science and Engineering, Tianjin University, Tianjin 300072, China*

^c *Collaborative Innovation Center of Chemical Science and Engineering (Tianjin), Tianjin 300072, China.*

^d *National Key Laboratory of Biochemical Engineering, Institute of Process Engineering, Chinese Academy of Sciences, Beijing 100190, China.*

[†] *J. F. Shi and S. H. Zhang contributed equally and shared the first authorship.*

E-mail: zhyjiang@tju.edu.cn; Fax: 86-22-23500086; Tel: 86-22-27406646

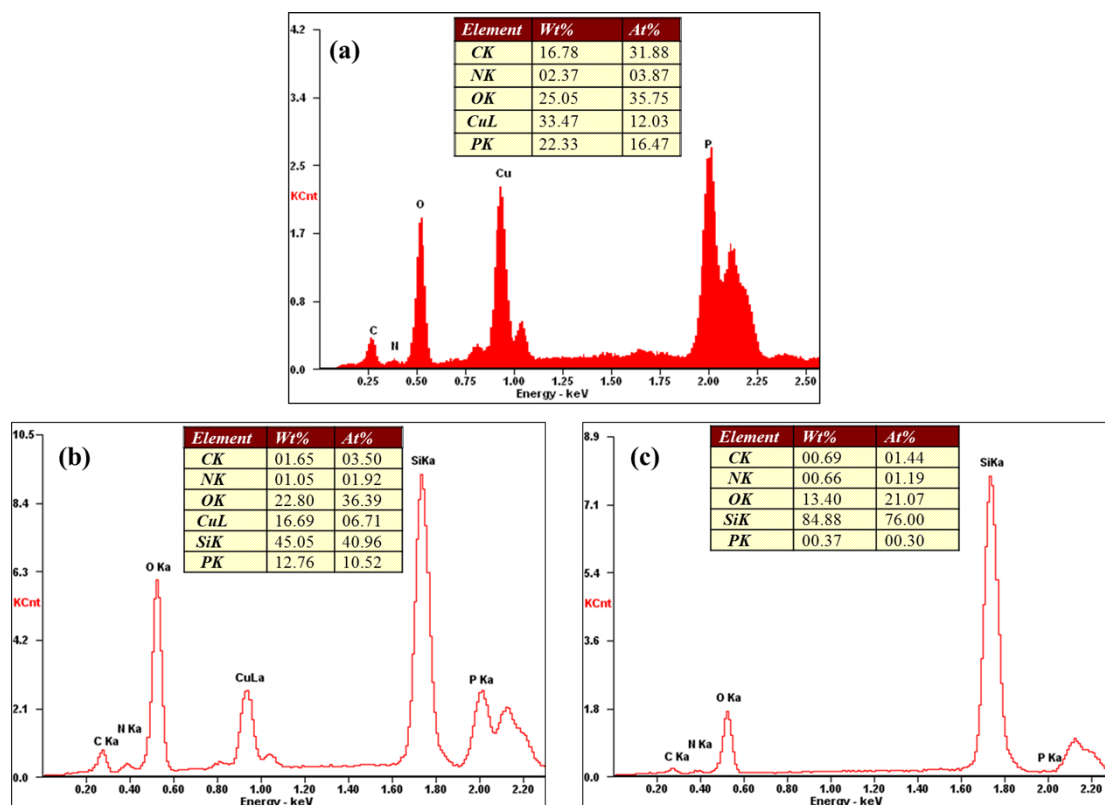


Figure S1. EDS curves of (a) CAT-Cu₃(PO)₂ microflowers, (b) (protamine/silica)₂ bilayers-coated microflowers, and (c) FPSH microcapsules.

As shown in **Figure S1a**, the EDS curve shows that P, N, O and Cu elements can be found in the CAT-containing microflower templates. Amongst, all N element, partial O element, and trace P element should be assigned to CAT, whereas all Cu element, most P element, and partial O element should be from the inorganic component of the microflower templates.

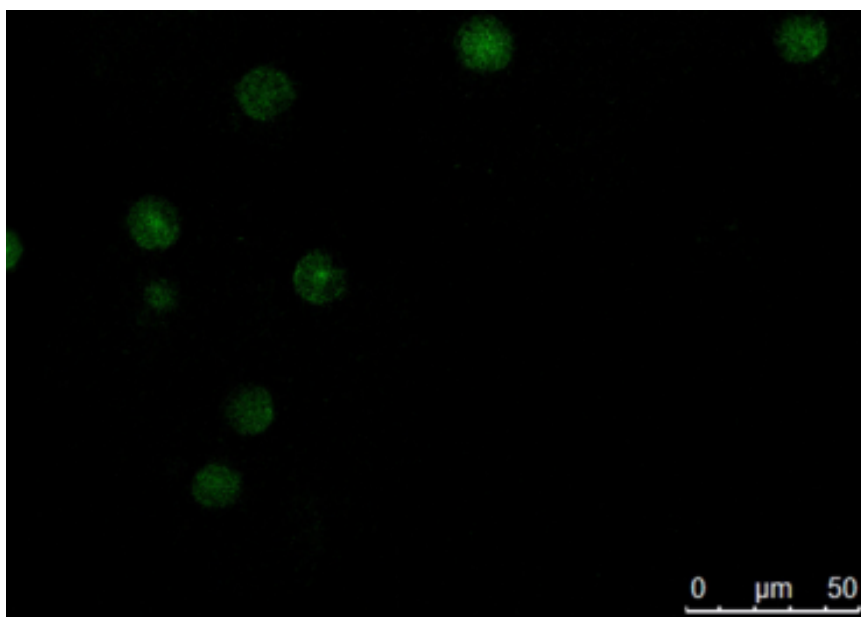


Figure S2. CLSM image of FPSH microcapsules. (*Herein, FITC-labeled CAT was utilized for synthesizing FPSH microcapsules in order to observe the location and distribution of enzymes in the capsules.*)

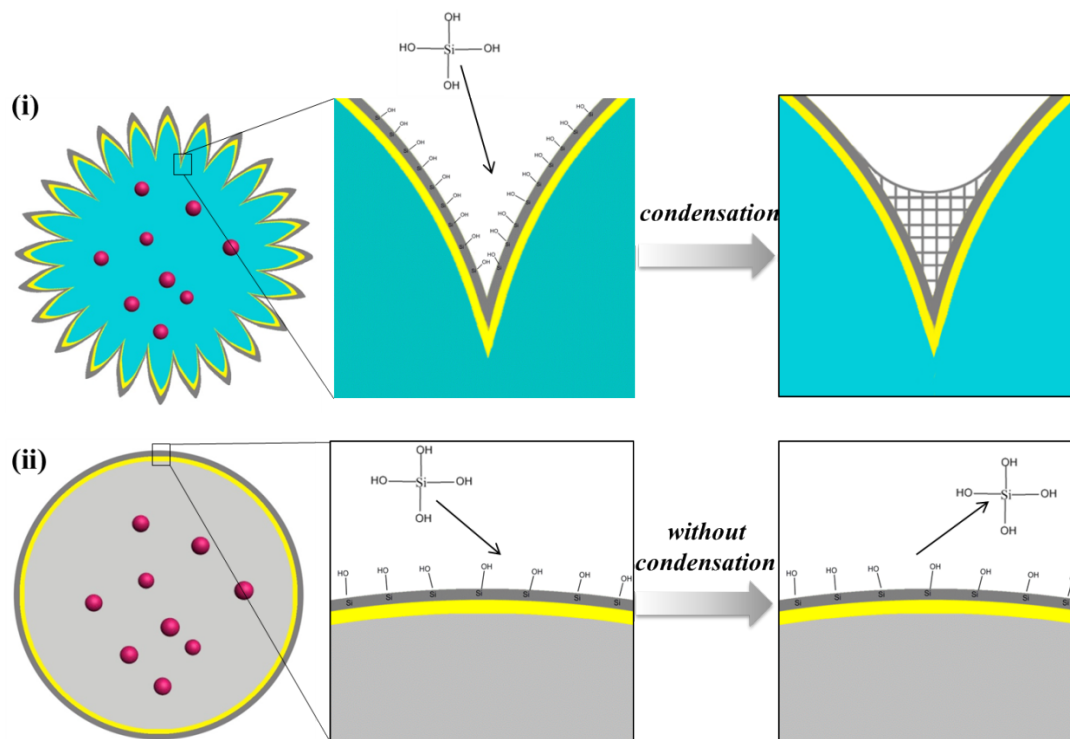


Figure S3. i) Silica network formed in the corner between two petals of FPSH microcapsules, and ii) no silica network formed on the surface of PSH microcapsules.

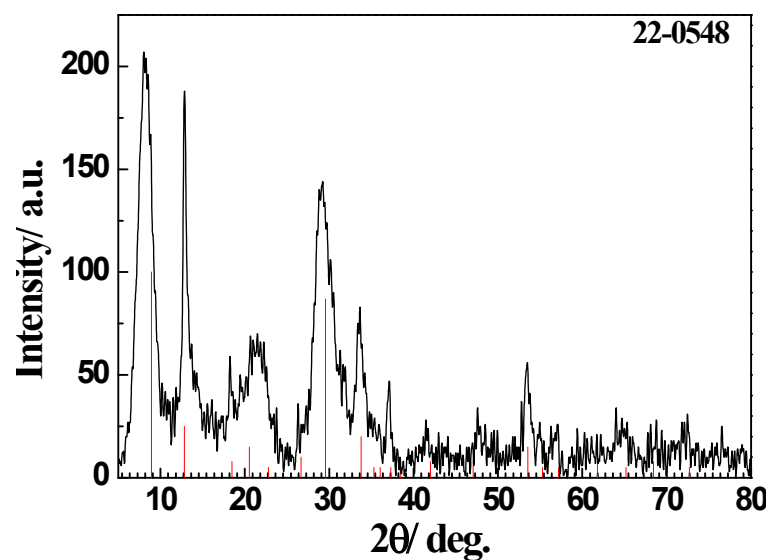


Figure S4. XRD pattern (black curve) of the CAT-containing microflower templates. Herein, the red line in this **Figure** is the standard crystal pattern of $\text{Cu}_3(\text{PO}_4)_2 \cdot 3\text{H}_2\text{O}$ (PDF-# 22-0548).

The XRD pattern of the CAT-containing microflower templates (**Figure S4**) fit well with the standard crystal pattern of $\text{Cu}_3(\text{PO}_4)_2 \cdot 3\text{H}_2\text{O}$ (PDF-# 22-0548). ^[1]

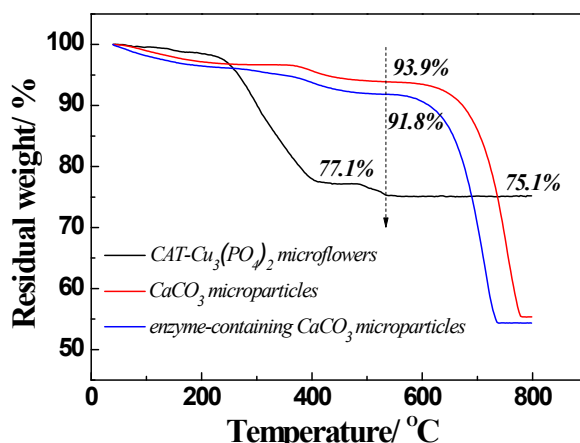


Figure S5. TGA curves of CAT-Cu₃(PO₄)₂ microflowers, CaCO₃ microparticles and enzyme-containing CaCO₃ microparticles.

In **Figure S5**, as the temperature increases from room temperature to 420 °C, the weight loss of CAT-Cu₃(PO₄)₂ microflowers is *ca.* 22.9 %, which is mainly due to the evaporation of free and bound water. Besides, the weight loss further increases to 24.9% as the temperature increases from 420 °C to 540 °C, which is primarily caused by the decomposition of CAT. The mass fraction of enzyme loading in the CAT-Cu₃(PO₄)₂ microflowers is *ca.* 2.0%.

Meanwhile, in the present study, during the synthesis of enzyme-containing CaCO₃ microparticles, poly (sodium styrenesulfonate) (PSS) is added and utilized to stabilize the structure of microparticles. Therefore, TGA curves of CaCO₃ microparticles and enzyme-containing CaCO₃ microparticles are both characterized for calculating the mass fraction of enzyme loading in the enzyme-containing CaCO₃ microparticles. Specifically, as shown in **Figure S5**, for both CaCO₃ microparticles and enzyme-containing CaCO₃ microparticles, when the temperature increases from room temperature to 420 °C, the weight loss is attributed to the evaporation of water. With

the temperature further increase to 540 °C, the organic components are completely decomposed and the residual weight of CaCO₃ microparticles and enzyme-containing CaCO₃ microparticles is 93.9 % and 91.8 %, respectively. The mass fraction (w , %) of enzyme loading in enzyme-containing CaCO₃ microparticles can be obtained from the following equation:

$$(1-w) * (1-93.9\%) + w = (1-91.8\%) \quad (S1)$$

After calculation, w is *ca.* 2.2%, which is similar to that of enzyme loading in the CAT-Cu₃(PO₄)₂ microflowers (2.0%).

Hence, minor differences could be obtained for the amount of enzyme loaded between CAT-Cu₃(PO₄)₂ microflowers and enzyme-containing CaCO₃ microparticles. In addition, a sharp decrease could be found as the temperature is over 650 °C, which is probably due to the decomposition of CaCO₃.

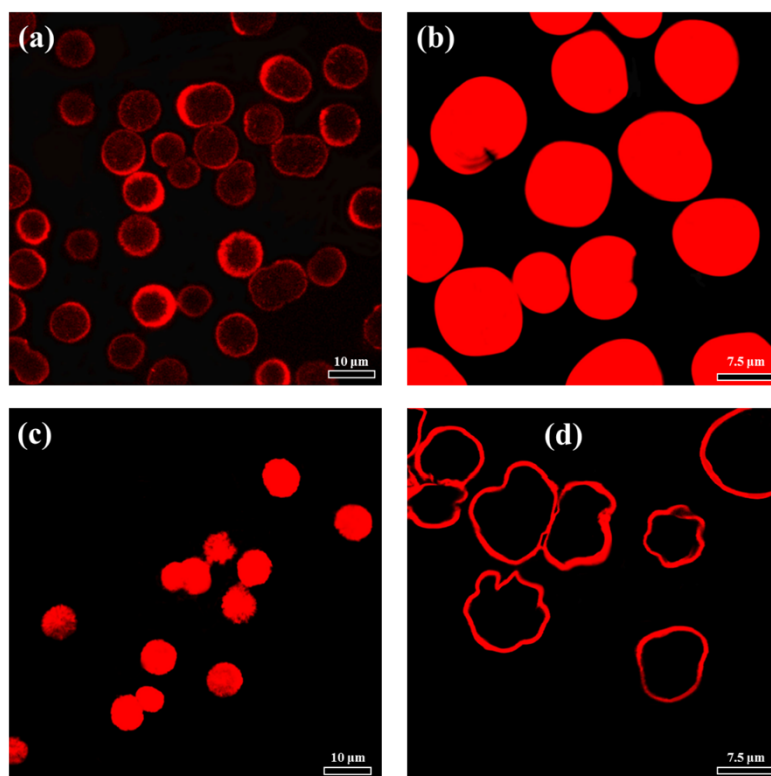


Figure S6. CLSM images of (a) CAT-Cu₃(PO₄)₂ microflowers, (b) enzyme-containing CaCO₃ microparticles, (c) FPSH microcapsules, and (d) PSH microcapsules adsorbed with rhodamine B.

In the present study, rhodamine B is utilized as the fluorescent molecule for investigating the adsorption behavior of all the four samples. After immersed in rhodamine B aqueous solution (0.01 mg ml⁻¹) for 10 min, the samples are collected and washed with water twice. As shown in **Figure S6a** and **S6b**, the CAT-Cu₃(PO₄)₂ microflowers exhibit strong fluorescent intensity on their surface and weak fluorescent intensity from the interior, while the enzyme-containing CaCO₃ microparticles exhibit uniform fluorescent intensity. The phenomenon indicates that rhodamine B molecules can diffuse into the interior of the CaCO₃ microparticles and stay on the outer surface of the microflowers. However, the fluorescent intensity

uniformly distributed on the FPSH microcapsules while mainly stay on the wall of the PSH microcapsules (**Figure S6c** and **S6d**). It indicates that rhodamine B can diffuse into the FPSH microcapsules but only stay on the wall of PSH microcapsules, which further verifies the strong adsorption capacity of the FPSH microcapsules.

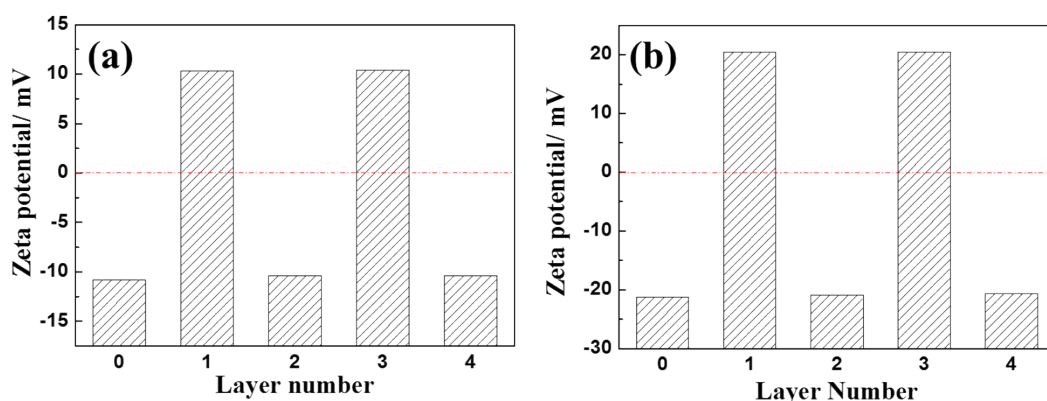


Figure S7. Surface zeta potential as a function of layer number for (a) CAT-Cu₃(PO₄)₂ microflowers, and (b) enzyme-containing CaCO₃ microparticles coated with protamine/silica layers. Layer 0 represented the surface zeta potential of pristine CAT-Cu₃(PO₄)₂ microflowers and enzyme-containing CaCO₃ microparticles.

To monitor the LbL process, we have measured the surface zeta potential of the CAT-Cu₃(PO₄)₂ microflowers and enzyme-containing CaCO₃ microparticles after the deposition of each protamine/silica layer according to previous method^[2]. As shown in **Figure S7a**, the switching of the zeta-potential between 10 mV and -10 mV indicates the alternative deposition of protamine and silica on the CAT-Cu₃(PO₄)₂ microflowers. In addition, a similar switch phenomenon between 21 mV and -21 mV are also observed for enzyme-containing CaCO₃ microparticles coated with protamine/silica layers (**Figure S7b**), implying the successful deposition of protamine and silica on the enzyme-containing CaCO₃ microparticles.

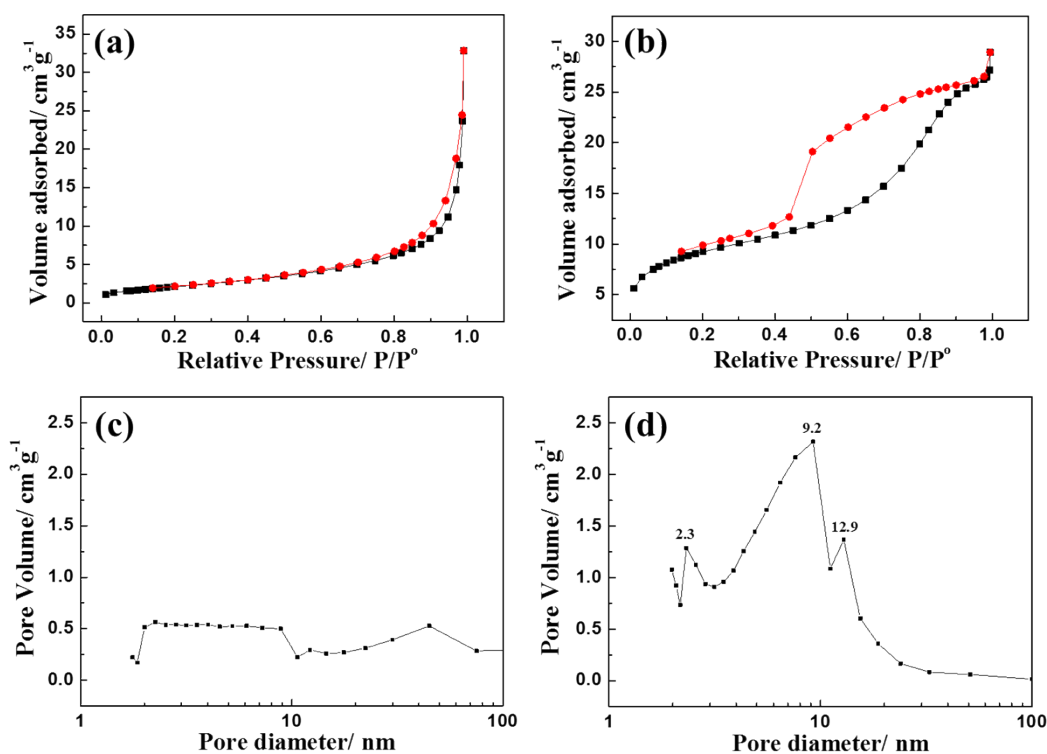


Figure S8. Nitrogen adsorption-desorption isotherms and pore size distribution curves by the BJH (Barrett-Joiner-Halenda) method of (a, c) microflowers, and (b, d) enzyme-containing CaCO₃ microparticles.

The nitrogen adsorption-desorption isotherms of CAT-Cu₃(PO₄)₂ microflowers, and enzyme-containing CaCO₃ microparticles are conducted. In **Figure S8a**, it can be observed that the isotherm of microflowers displays a kind of hysteresis loop, which does not level off at relative pressures near the saturation vapor pressure. It can be assigned to Type H3 according to IUPAC recommendations, indicating the presence of a highly interconnected and slit-shaped pore structure. As shown in **Figure S8b**, the isotherm of enzyme-containing CaCO₃ microparticles displays a hysteresis loop with triangular shape and steep desorption branch, which can be assigned to Type H2 according to IUPAC recommendations. This kind of hysteresis loop is often observed

in many porous inorganic oxide materials, indicating the presence of pores with narrow mouths (ink-bottle pores). The BET surface area and pore volume are $7.84 \text{ m}^2 \text{ g}^{-1}$ & $0.051 \text{ cm}^3 \text{ g}^{-1}$ for microflowers, and $32.93 \text{ m}^2 \text{ g}^{-1}$ & $0.047 \text{ cm}^3 \text{ g}^{-1}$ for enzyme-containing CaCO_3 microparticles. In addition, the pore size distribution for both two samples is different. The pore size of enzyme-containing CaCO_3 microparticles is primarily located at *ca.* 9.2 nm (**Figure S8c**); while rare pores can be found in $\text{CAT-Cu}_3(\text{PO}_4)_2$ microflowers (**Figure S8d**).

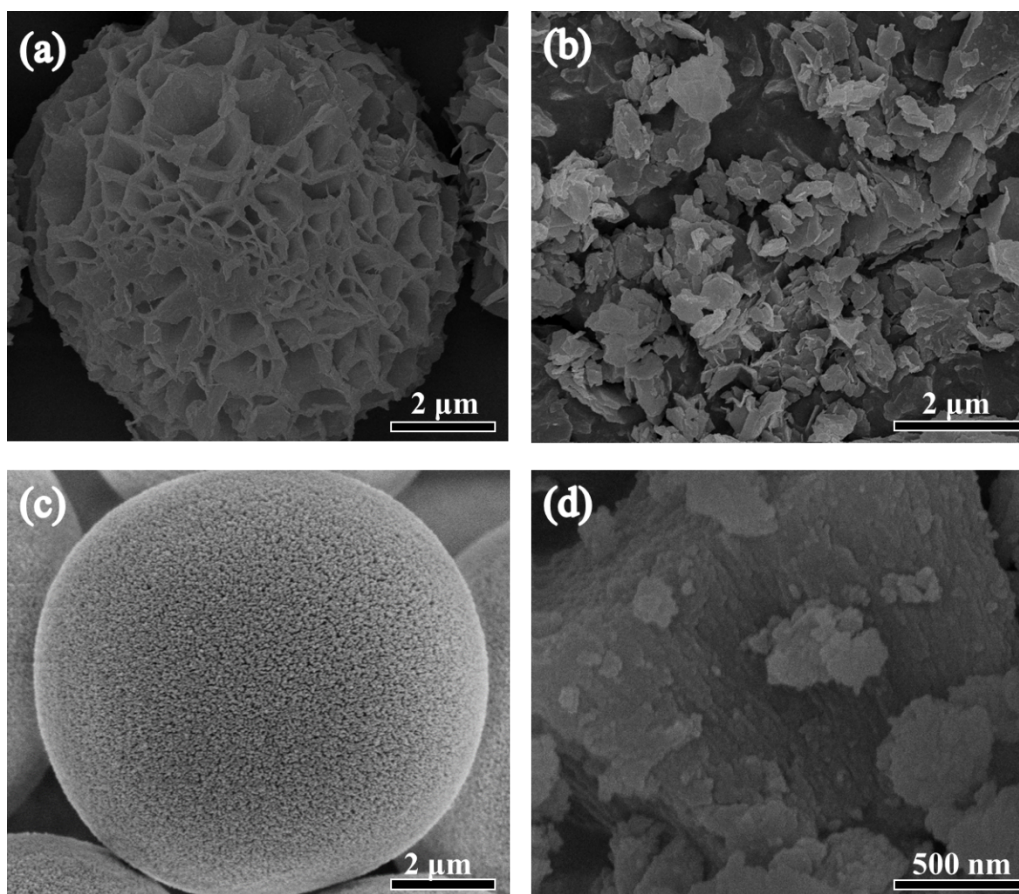


Figure S9. High magnification SEM images of (a) microflowers, (b) mechanically ruptured CAT-Cu₃(PO₄)₂ microflowers, (c) enzyme-containing CaCO₃ microparticles, and (d) mechanically ruptured enzyme-containing CaCO₃ microparticles.

Since the topological structures of the capsule wall are directly influenced by the templates, it's critical to demonstrate the structure of templates clearly. **Figure S9a** showed a typical structure of contact CAT-Cu₃(PO₄)₂ microflowers, where a collection of petals were homogeneously distributed on the surface. By contrast, the enzyme-containing CaCO₃ microparticles exhibit a spherical shape with a smooth surface (**Figure S9c**). To further clarify the structure of two kinds of the templates, CAT-Cu₃(PO₄)₂ microflowers and enzyme-containing CaCO₃ microparticles are

mechanically ruptured. Obviously, there are many flakes as shown in **Figure S9b**, which further proves that CAT-Cu₃(PO₄)₂ microflowers are the aggregation of petals. Moreover, as illustrated in **Figure S9d**, a typical cross-sectional image of the enzyme-containing CaCO₃ microparticles can be observed. And numerous nanoparticles are considered to be aggregated into the CaCO₃ microparticles^[3]

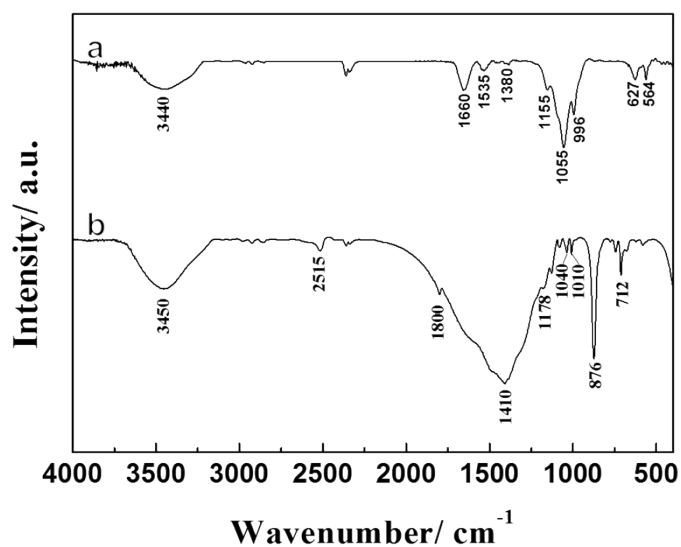


Figure S10. FTIR spectra of (a) CAT-Cu₃(PO₄)₂ microflowers, and (b) enzyme-containing CaCO₃ microparticles.

The FT-IR spectra for the CAT-Cu₃(PO₄)₂ microflowers and enzyme-containing CaCO₃ microparticles are also provided as shown in **Figure S10**. Specifically, in **Figure S10a**, the absorption bands at 627 cm⁻¹ and 564 cm⁻¹ are attributed to the ν_4 O-P-O bending vibrations and the composed bands between 1200 cm⁻¹ and 996 cm⁻¹ are mainly resulted from the ν_3 P-O stretching vibration, indicating the existence of phosphate.^[4] The absorption bands at 3440 cm⁻¹, 1660 cm⁻¹, 1535 cm⁻¹ and 1380 cm⁻¹ are the typical bands of amide, which confirms the hybrid composition of the microflowers. By contrast, **Figure S10b** shows the FTIR spectrum of enzyme-containing CaCO₃ microparticles. The absorption bands at 2515 cm⁻¹, 1410 cm⁻¹, 876 cm⁻¹ and 712 cm⁻¹ correspond well with CO₃²⁻ ion.^[5] Meanwhile, the absorption band at 1040 cm⁻¹ is assigned to the sulfonic group symmetric-stretching vibration, suggesting the existence of PSS in the enzyme-containing CaCO₃ microparticles.^[6]

Besides, we also found the absorption band belonging to amide of CAT at *ca.* 3450 cm^{-1} .

Table S1. Zeta potential of CAT-Cu₃(PO₄)₂ microflowers and enzyme-containing CaCO₃ microparticles.

Samples	Zeta potential/ mV
CAT-Cu ₃ (PO ₄) ₂ microflowers	-10.8
Enzyme-containing CaCO ₃ microparticles	-21.2

As shown in **Table S1**, the zeta potential of the CAT-Cu₃(PO₄)₂ microflowers and enzyme-containing CaCO₃ microparticles are, respectively, -10.8 mV and -21.2 mV, which may avoid the aggregation of the particles for their electrostatic repulsion.

Cost accounting

In this study, the enzyme encapsulation efficiency during the synthesis of CAT- $\text{Cu}_3(\text{PO}_4)_2$ microflowers is ~30% (*data not shown in the original manuscript*). However, it can be found that the phosphate is much excess, and CuSO_4 can be completely consumed during the synthesis process of microflowers. Therefore, the other 70% amount of enzyme can be reuse through repeating the microflower-generation process by adding appropriate amount of enzyme and CuSO_4 into the excess phosphate buffer solution. Finally, the waste of enzyme during the immobilization process can be ignored.

Moreover, as illustrated in the manuscript, the loading capacity of enzyme in the microflowers is about 35.1 mg g^{-1} . And the enzyme that is utilized for conducting the catalytic reaction is ~0.1 mg for both FPSH microcapsules and free enzymes. Therefore, the amount of carrier, that is the $\text{Cu}_3(\text{PO}_4)_2$ can be considered to be ~2.8 mg. Correspondingly, the amount of CuSO_4 and phosphate buffer (*both precursors*) is 0.0186 mmol and 0.0279 mmol, respectively. Since the unit price of $\text{CuSO}_4 \cdot 5\text{H}_2\text{O}$, $\text{NaH}_2\text{PO}_4 \cdot 2\text{H}_2\text{O}$ and $\text{Na}_2\text{HPO}_4 \cdot 12\text{H}_2\text{O}$ is, respectively, RMB 68.00, 39.00 and 39.00 yuan/(500g), the cost of these three reagents for fabricating 2.8 mg $\text{Cu}_3(\text{PO}_4)_2$ would be RMB 0.00060, 0.00017 and 0.00039 yuan, respectively. Combining with the cost of 0.1 mg CAT (RMB 300 yuan/g), the total cost for fabricating the microflowers with 0.1 mg enzymes would be RMB 0.03116 yuan.

Moreover, the H_2O_2 conversion of FPSH microcapsules is only ~40% that of free enzymes under a 3-min reaction period. Taking the H_2O_2 conversion of free enzymes as 1, the H_2O_2 conversion of FPSH microcapsules for each cycle is 0.400, 0.344, 0.304, 0.244, 0.192, 0.140 and 0.108, respectively. After calculation, the total H_2O_2

conversion of FPSH microcapsules would be 1.732, which is much lower than that of free enzymes (7.000). Moreover, as mentioned above, the cost of catalysts after the 7th reaction process is RMB 0.03116 and 0.21 yuan for FPSH microcapsules and free enzymes, respectively. **Consequently, to convert one unit of H₂O₂, the cost of catalysts is 0.018 and 0.03 yuan for FPSH microcapsules and free enzymes, respectively.**

Reference:

1. J. Ge; J. Lei; R. N. Zare, Protein-inorganic hybrid nanoflowers. *Nature Nanotechnology* **2012**, 7 (7), 428-432.
2. X. D. Li, Q. L. Hu, L. H. Yue, J. C. Shen, Synthesis of size-controlled acid-resistant hybrid calcium carbonate microparticles as templates for fabricating “micelles-enhanced” polyelectrolyte capsules by the LBL technique, *Chemistry-A European Journal* **2006**, 12(22), 5770-5778.
3. G. B. Sukhorukov; D. V. Volodkin; A. M. Günther, Porous calcium carbonate microparticles as templates for encapsulation of bioactive compounds. *Journal of Materials Chemistry* **2004**, 14(14), 2073-2081.
4. A. Stoch; W. Jastrzebski; A. Brozek, FTIR absorption-reflection study of biomimetic growth of phosphates on titanium implants. *Journal of Molecular Structure* **2000**, 555, 375-382.
5. H. A. Al-Hosney; V. H. Grassian, Water, sulfur dioxide and nitric acid adsorption on calcium carbonate: A transmission and ATR-FTIR study. *Physical Chemistry Chemical Physics* **2005**, 7(6), 1266-1276.
6. J. Jang; J. Ha; J. Cho, Fabrication of Water-Dispersible Polyaniline-Poly(4-styrenesulfonate) Nanoparticles For Inkjet-Printed Chemical-Sensor Applications. *Advanced Materials* **2007**, 19(13), 1772-1775.